Proceedings of the 16th European Turbomachinery Conference (ETC16)
Turbomachinery, Fluid Dynamics and Thermodynamics,
March 24-28, 2025, Hannover, Germany

Impact of Turbine Inlet Temperature Distortion on Rotor Blade Heat Transfer at Engine Representative Conditions Using Infrared Thermography

Manuela Sisti[1], Richard S. Adoua[2], Chiara Falsetti[2*], Haidong Li[2], and Paul F. Beard[1]

[1]Department of Engineering Science, University of Oxford, Oxford, OX2 0ES, UK
[2] Rolls-Royce PLC, Filton, Bristol BS34 7QE, UK
[2*]Department of Aerospace Engineering, Delft University of Technology, Postbus 5, 2600 AA Delft, The Netherlands

Abstract

With inlet gas temperatures of high-pressure turbine stages of engines reaching almost 2000 K, shroudless turbine blade tips have become a performance and life critical component. As temperature distortions have a direct impact on rotor blades heat transfer, there is a need to gain experimental insights with highly engine representative conditions. This paper presents heat transfer measurements, scaleable to engine conditions, from a rotating transonic turbine test facility using a novel infrared measurement technique [1]. Experiments were conducted in the Oxford Turbine Research Facility (OTRF), a rotating facility capable of matching engine Mach and Reynolds numbers, non-dimensional speed and gas-to-wall temperature ratio. The work investigates the effect of a temperature profile typical of a rich burn combustor in a modern civil engine on the heat transfer in the high-pressure turbine rotor. Two inlet conditions are investigated: (1) uniform temperature and pressure distribution, and (2) radial temperature and uniform pressure distribution. The single stage high-pressure turbine includes cooled nozzle guide vanes and uncooled rotor blades with a squealer tip geometry. High-resolution two-dimensional transient measurements of surface temperature are conducted using infrared thermography, processed to heat flux and used to determine adiabatic wall temperature and Nusselt number for the blade tip and pressure side, a result not achieved before. Comparison to thin-film gauge heat transfer measurements on the blade pressure surface highlight the capabilities of the infrared thermography system. A computational simulation conducted using the Rolls-Royce code HYDRA is used to demonstrate the confidence in the novel experimental measurements.

Keywords: infrared thermography, high-pressure turbine, combustor turbine interaction, temperature distortion, heat transfer.

1 Introduction

It is well understood that increasing the turbine entry temperature increases thermodynamic efficiency, and consequently a reduction in specific fuel consumption. Since 1950, the turbine entry temperature has risen from approximately 1000 K to almost 2000 K in current in-service engines [2]. Thus, the high-pressure (HP) turbine stage operates under heat loads that could compromise the integrity of the components, possibly leading to burnout [3]. The heat loads on the most critical part, the HP blade tip, is further exacerbated by the presence of a clearance gap (tip clearance) between the rotating blade and static casing. The tip clearance, typically less than 1% of the blade span for large engines increasing to 1.5% for smaller engines [4], is necessary to avoid the blade rubbing and to allow for blade growth caused by centrifugal forces and temperature expansion. However, this gap allows fluid to leak over the blade tip from the pressure to the suction side, driven by the strong pressure gradient across the tip. This flow, commonly referred to as tip leakage, is the primary cause of high thermal loading on the blade tip [4] [5] [6], as well as contributing to turbine aerodynamic losses [7], [8], [9]. To further complicate things, the blade tip can be eroded as the engine accumulates flight hours, leading to an increased effective tip gap and to a higher leakage mass flow rate compared to a sharp-edge tip at the beginning of the engine's operational life [10].

One typical strategy to reduce leakage flow, is the use of squealer tip geometries, including a thin rim that runs around both pressure and suction sides, that increases the flow resistance for a given pressure difference across the tip.

The nature of the leakage flow in a squealer tip geometry, depicted in Figure 1, is strongly three dimensional with multiple interacting vortices. First, a separation vortex is generated as the incoming flow separates from the inner edge of the pressure-side rim. This vortex follows the pressure surface sidewall and exits near the blade trailing edge. Depending on the size of the cavity, a reattachment region may form. A separation vortex also originates from the stagnation region and extends over the blade suction surface. Other vortices are generated as the flow exits the suction side rim which travels down the blade suction surface potentially interacting with the blade secondary flow vortices.

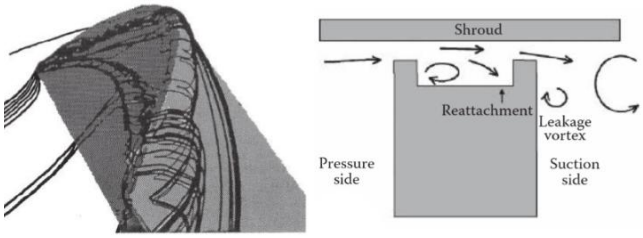

(a) (b)

Figure 1 – Leakage flow over an unshrouded squealer tip blade, including: (a) typical flow patterns from [11], and (b) conceptual representation from [11].

Several authors have demonstrated that grooved tip designs are beneficial in reducing heat transfer due to leakage flow compared to a flat tip geometry. Metzger et al. [4] and Chyu et al. [12] were among the first to study the heat transfer in a

*Corresponding author: paul.beard@eng.ox.ac.uk, tel. +44 1865 288 760

Paper ID: ETC2025-318

rectangular cavity as a stationary model of a grooved turbine blade tip. Both studies showed reduced heat transfer at the upstream end of the cavity compared to a flat tip. In contrast, higher heat transfer coefficients were observed at the downstream end due to flow reattachment inside the cavity. Additionally, as the groove depth increased, the heat transfer on the cavity floor decreased, due to the formation of a whole recirculation vortex which prevented the reattachment region. Heyes et al. [13] studied the impact of suction side squealer and pressure side squealer on leakage flow against a flat tip, showing the beneficial effect of squealer, particularly the suction side. Azad et al. [14] [15] identified different heat transfer region on the cavity surface of a squealer tip blade compared to a flat tip blade, under varying tip gaps. Despite a higher heat transfer on the rim surface and localised regions of heat transfer enhancement, the authors overall concluded that the squealer tip exhibited a lower heat-transfer coefficient when compared to the flat tip case. Kwak et al. [16] drew similar conclusions.

The bulk of experimental studies on tip leakage flow have been conducted in low speed wind tunnel and linear cascades, primarily due to the challenges of instrumenting rotor blades in engine-representative facilities. Only a limited number of studies on tip heat transfer have accurately simulated the engine environment, including high-speed rotation. Didier et al. [17] at the von Karman Institute investigated the heat transfer of a flat tip blade in a compression tube test rig with a full-scale rotating turbine stage. The facility simulated Reynolds and Mach numbers, as well as gas/wall and gas/coolant temperature ratios of modern aero engine HP turbines. Dunn and Haldeman [18] at the Ohio State University examined the heat transfer of a squealer tip blade in a shock-tunnel, housing a full-scale rotating turbine with transonic vane exit conditions. Their setup operated at design flow function, total to static pressure ratio, corrected speed, and wall to total temperature ratio. Both studies adopted Nusselt number distributions referenced to a gas temperature rather than adiabatic wall temperature, not allowing direct non-dimensional scaling to engine conditions. Didier et al. [17] used 24 thin-film gauges around the pressure and suction sides at the hub and at 15, 50, and 85% span, along with just five gauges on the tip. Dunn and Haldeman [18] instrumented the pressure side, suction side, and platform with sufficient gauge density to reconstruct a spatial Nusselt distribution. However, tip instrumentation was limited, with only three gauges on the tip cavity, three on the pressure side rim, and two on the suction side rim. Thorpe et al. [19] at the University of Oxford studied heat transfer on a flat tip in a transonic turbine stage test facility, improving spatial resolution by using 17 thin-film gauges on the tip and presented the unsteady heat transfer rate derived from those measurements.

All of these studies relied on point-based instrumentation. The first study to produce fully resolved spatial data in a transonic rotating facility was conducted by Christensen et al. [20] at Ohio State University. The authors used IR thermography to study the heat transfer of a cooled squealer tip blade and presented data in terms of Stanton number. Measurements covered only a small section of the blade tip at mid chord, and again referenced Stanton number to a gas temperature rather than adiabatic wall temperature.

To fully understand the heat transfer on the blade tip in real engine environment, temperature distortions at the inlet to the HP turbine must also be simulated. The flow exiting the combustor of a modern engine is characterized by large spatial and temporal temperature distortions [21]. Tip burnout mechanism is typically worse at the rear half of the rotor tip particularly towards the pressure side. This could be explained by considering the presence of temperature distortion, so called “hot streaks” from the combustor, generally the result of the presence of distinct burners, with a significant radial temperature distribution caused as dilution jet cooling is employed to protect the combustor walls from extreme temperatures. However, very few turbine facilities have the capability to simulate temperature distortions.

In 2009, Povey and Qureshi [22] discussed the various definitions used to quantify temperature distortions in literature and compared six experimental turbine facilities capable of generating radial and circumferential temperature profiles.

The first measurements of blade surface temperature with inlet temperature distortion were reported by Shang et al. [23] using thin film double-sided heat transfer gauges mounted around the blade pressure and suction sides. The authors also conducted a simulation for the experiments (Shang and Epstein [24]) to analyse the impact of hot streaks on the blade heat load. The authors confirmed Butler et al.’s [25] findings, observing that a radial distortion in temperature distribution strongly affected the blade heat transfer, particularly for tip and hub. Affected by buoyancy forces and enhanced rotor secondary flows, migration of hot gas towards the tip and the hub regions can significantly increase heat transfer.

Extensive research on turbine stage heat transfer with inlet temperature distortion has been conducted at the Oxford Turbine Research Facility. Chana and Jones [26] reported measurement of heat transfer on casing and tip of an unshrouded turbine stage with and without temperature distortion at turbine inlet. Rotor casing Nusselt number was spatially resolved from surface temperature measurements using thin film heat-flux gauges, while just three gauges were mounted on the tip providing localised measurement of Nusselt number (referenced to gas temperature). A reduction of casing heat load was reported with inlet temperature distortion. Beard et al. [27] measured a turbine efficiency deficit of -0.28% with the introduction of a more pronounced radial and circumferential temperature profile, driven by increased losses in the rotor passage. Qureshi et al. [28] investigated the effect of the updated inlet distortion on rotor heat transfer. CFD simulations confirmed that heat flux changes were driven by changes in adiabatic wall temperature rather than heat transfer coefficient.

It can be concluded that temperature uniformities at the inlet to the high-pressure turbine, typical of real engine operations, strongly affect both the aerodynamics and heat transfer to the rotor blades. Several studies have investigated the physics of hot-streak migration. However, most heat transfer experimental data gathered at engine-representative conditions focus on the casing heat transfer, whilst rotor blade heat transfer has been spatially resolved only in cascade facilities.

The aim of this paper was to investigate the effect of a rich combustor exit temperature profile on the heat transfer of an unshrouded high-pressure turbine blade with a squealer tip geometry at engine representative conditions in a rotating transonic facility. This paper presents the first experimental spatially resolved evaluation of adiabatic wall temperature on a rotor blade in such a facility, used to define a Nusselt

number that can be scaled to engine conditions. The capability of such measurements are compared with traditional point-based thin film measurements. Finally, validated computational results are presented to give confidence to the measurements. To the best of the authors' knowledge, such measurements, acquired with an infrared (IR) camera, have not been reported before.

2 Experimental Setup

Experiments were conducted in the Oxford Turbine Research Facility (OTRF), a transient rotating facility designed for engine representative investigations. A review of recent work conducted in the OTRF can be found in [29]. A schematic of the facility is shown in Figure 2. Prior to a run, the plug valve is closed, the test section is evacuated to approximately 10 mbar, and the turbine rotor is spun to the design speed. Simultaneously, the main test gas undergoes isentropic compression within the piston tube, as high-pressure air is injected into the pump tube behind the piston. When the desired pressure and temperature are reached, the fast-acting plug valve is opened, allowing the mainstream to flow into the test section. Cooling flows, all at ambient temperature, are initiated prior to the mainstream and metered by independent sonic venturi nozzles. In this study, the SILOET single stage high-pressure turbine was installed in the facility [30], consisting of 40 cooled nozzle guide vanes and 60 uncooled transonic rotor blades – see Figure 3. The vane includes ten rows of film cooling and trailing edge slot ejection. The rotor blade includes a squealer tip geometry.

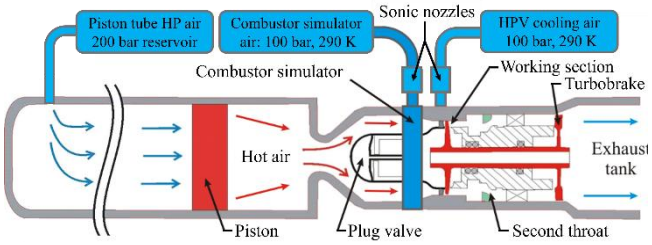

Figure 2 – Schematic of the OTRF [31].

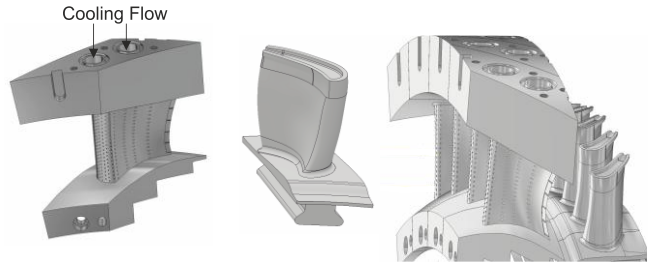

Figure 3 – SILOET turbine

2.1 Radial Temperature Distribution Generator

The Oxford Turbine Research Facility is equipped with a combustor simulator, which enables simulation of time-average velocity and temperature profiles typical of both rich and lean-burn combustors [32].

A sectional view of the combustor simulator configuration used in the present investigation is shown Figure 4. The setup enabled simulation of the temperature profile downstream of a rich burn combustor in a modern civil engine, which shows a large radial temperature variation with little swirl. In this configuration, a swirler plate used to generate vortices typically of lean-burn systems, is replaced by a turbulence generation grid of radial rods.

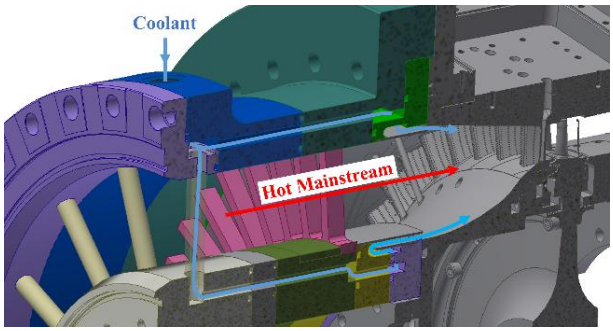

Figure 4 – Sectional view of combustor simulator showing coolant and hot mainstream mixing.

The desired temperature field at NGV inlet is achieved by injecting ambient temperature air from hub and casing annular slots upstream of the NGV inlet contraction, allowing the flow to mix with the hot mainstream flow. Extensive measurements to characterise the Radial Temperature Distortion Factor (RTDF) used in this study are reported by Singh et al. [33]. The measured temperature field is shown in Figure 5 in terms of non-dimensional total temperature effectiveness, defined as $T_{0,eff} = (T_{01} - T_{0c})/(T_{0h} - T_{0c})$. The two-dimensional map of the temperature profile shown in Figure 5(a) was measured at 264 locations on a plane located 1½ NGV axial chords upstream of the NGV leading edge using thermocouple rakes spread across two NGV pitches and covering approximately 4% to 98% of the radial span. As desired, the measured profile shows a predominantly radial variation, with the target and measured circumferentially averaged RTDF profiles, shown in Figure 5(b), matching both in magnitude and form.

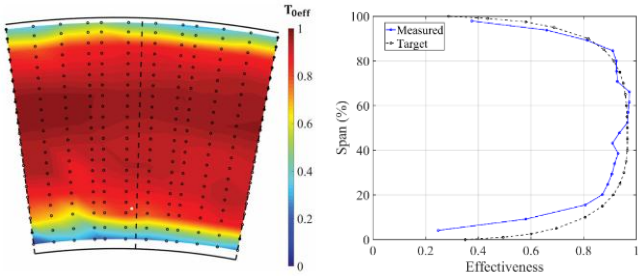

(a) (b)

Figure 5 – RTDF stage inlet total temperature: (a) Measured area-survey (thermocouple locations shown as circles); (b) Radial profile compared to target, both from [33].

The experiments presented in this study were conducted with two inlet conditions: uniform temperature T_{01} and pressure p_{01} distribution, and RTDF (with no swirl) and uniform pressure p_{01} distribution. With uniform inlet conditions, the combustor simulator has a passive role, with no RTDF coolant being injected, and the hot mainstream gas flowing into the turbine stage unperturbed.

It is important to note, that although the temperature profile at NGV inlet includes little circumferential variation, NGV film cooling and trailing edge slot coolant ejection results in a significantly larger circumferential variation of total temperature at NGV exit with RTDF compared to uniform inlet conditions, as shown by the CFD results from the case described by Singh et al. [34] in Figure 6.

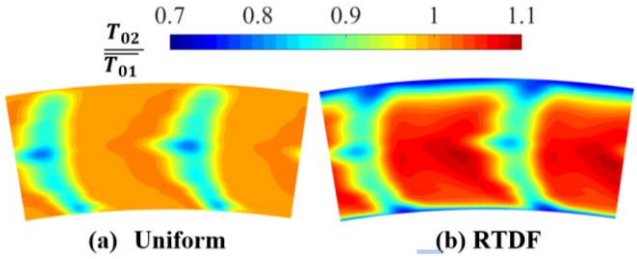

Figure 6 – Time-averaged NGV exit total temperature contours with (a) uniform inlet, and (b) RTDF from unsteady CFD described by Singh et al. [34].

Typical time traces of inlet total pressure and temperature, rotor exit static pressure, total-to-static pressure ratio and shaft speed for a OTRF test with the RTDF inlet condition are shown in Figure 7. Vacuum and ambient temperature conditions are observed at the beginning of each test. The vane and RTDF cooling flows are injected prior to the opening of the plug valve, seen in the pressure and temperature traces by a rise at t = 1.1 s and t = 1.7 s for the RTDF and NGV cooling respectively. The rise in total temperature is a result of isentropic compression. The plug valve opens at t = 2.43 s, and the inlet total pressure and temperature increase, reaching quasi-steady conditions at t = 2.60 s. The test run ends when the piston reaches the end of the piston tube at t = 2.9 s. As a result, the run window is approximately 300 ms. Throughout the run, the inlet total temperature mirrors the inlet total pressure almost isentropically.

The total-to-static stage pressure ratio is stable and equal to nominal value of 2.63 during the run. Similarly, the turbine rotor speed is approximately flat during the run, with a value

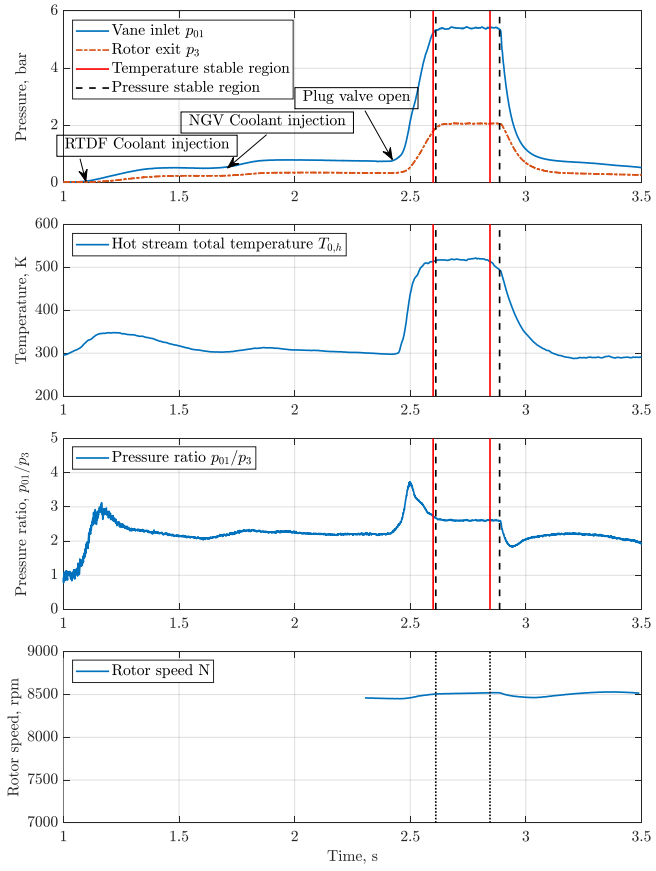

Figure 7 – Typical traces of stage pressures and temperatures for a OTRF test run with RTDF inlet conditions.

close to the design intent of 8500 rpm. The behaviour of a test with uniform inlet conditions is identical, omitting the influence of the RTDF coolant flow.

The NGV inlet total pressure is used to calculate the portion of the run which is aerodynamically stable. The same approach is used to find the temperature stable region in the run, in this case the temperature signal of the hot stream is used. In Figure 7, the pressure and temperature stable regions are individuated by dashed and solid vertical lines, respectively, and the start and finish of the run is defined as the smallest interval of the combination of both the pressure and temperature stable regions.

2.2 Infrared thermography and thin-film gauges instrumentation

For the first time, this paper presents complete surface maps of blade wall temperature, adiabatic wall temperature and Nusselt number measured in a transonic rotating turbine test facility such as the OTRF using infrared (IR) thermography. A detailed description of the measurement methodology is described by Sisti et al. [1], [35], [36] with further information specific to this study given here.

A FLIR A6751 SLS LWIR infrared camera was used to capture thermal images of the blade tip and pressure surfaces. The IR camera was synchronised to the blade rotation, capturing one image per revolution, and controlled using an NI sRIO FPGA digital inputs/outputs system. The block diagram and typical signals used for camera synchronisation and control are shown in Figure 8.

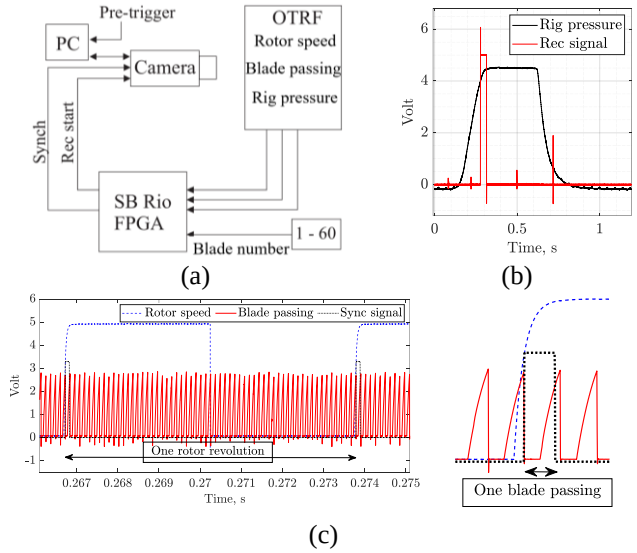

Figure 8 – Camera synchronisation and triggering system. (a) block diagram; (b) rig pressure and camera recording signals; (c) rotor speed, blade passing, camera sync signals.

The voltage signal from a pressure transducer measuring turbine inlet total pressure was used to create a digital pulse to trigger camera recording. These two signals are depicted in Figure 8(b). The camera record pulse, illustrated in red, was generated when the pressure transducer signal, illustrated in black, surpassed 4 V. The pre-trigger, necessary to record the entire time history of the experiment, was controlled through the camera software. The signals employed in the camera synchronisation are shown in Figure 8(c). The rotor speed in a typical run is depicted in blue, the maximum frequency is approximately 142 Hz, with an amplitude of 0 – 5 V. The

blade passing signal is depicted in red, the maximum frequency is approximately 8.5 kHz, with an amplitude of $0 - 2.5$ V. The rotor speed and blade passing signals are used to count the blades, and the synchronisation pulse is generated when the desired blade number is reached.

A photograph of the rotor configuration used in this study, as well as the schematic of the IR camera setup and typical field-of-view (FOV) for blade tip measurements are shown in Figure 9. The camera was mounted on a rail with a rotary mechanism, enabling the required inclination to focus on the blade pressure side. Optical access was achieved through a zinc selenide window, assembled in the overtip region. The blades allocated to IR measurements were coated with a semi-crystalline thermoplastic (polyether ether ketone – PEEK) to create a large surface temperature rise during the stable portion of the run, thus enabling regression to adiabatic wall temperature. With a thickness ranging between 2 and 3 mm, the substrate could be considered semi-infinite in the test time, according to the $x = \sqrt{\alpha t}$ rule [37]. Given its thermal diffusivity of 0.158 mms^{-1} and a test time of 0.5s, a minimum depth of 0.28 mm was required.

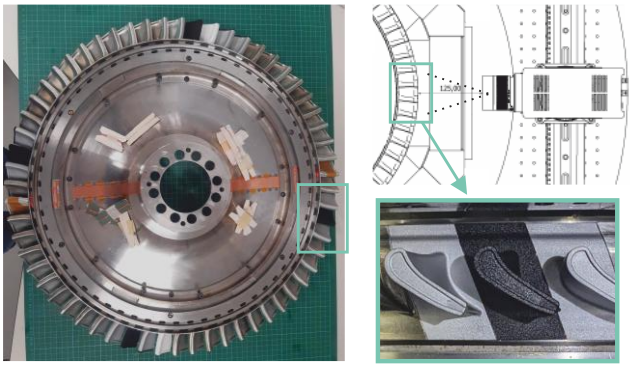

Figure 9 – OTRF rotor assembly including photograph of rotor, setup schematic and photograph of typical FOV for rotor tip IR thermography measurements.

The coated blades were sprayed with paints characterized by two opposite emissivity values: a black matt high emissivity paint, and aluminium low emissivity paint. This was required to allow the corrections of the reflected temperature in the infrared data.

Two of the blades in the rotor assembly were instrumented with single sided platinum thin-film heat transfer gauges. Gauges were installed at 80% span on blade suction and pressure surfaces. The gauges manufacturing procedure followed the technique presented by Collins et al. [38]. The instrumented blades underwent multiple cycles of annealing to enhance film's adhesion and to mitigate drift in the resistance of the platinum thin-film. The temperature coefficients of resistance were calibrated in a water bath. A slip-ring was used to transmit the signal from the thin-film gauges on the rotor to an in-shaft data acquisition system. Analogue signal condition is applied to the data prior to in-shaft storage, including high-frequency boost as described by Anthony et al. [39]. The in-shaft system also supplied the gauge current and allows data acquisition for approximately 4s at 1 MHz sample rate.

3 Experimental Results

The infrared data was processed to determine target temperature following the methodology presented by Sisti et al. [1] [40] [35]. Correction for emissivity of the target, surroundings reflectance, and transmittance of the optical path were applied following the block diagram shown in Figure 10**.** Two runs were used, with the camera focusing on a high emissivity blade in one run and a low emissivity blade in the other. After calculating the blackbody equivalent temperatures T_{cam1} and T_{cam2}, the two datasets were used alongside the calibrated emissivity values, the optical window calibrated transmittance, τ, and temperature, T_{opt}, to calculate the corrected target temperature T_t.

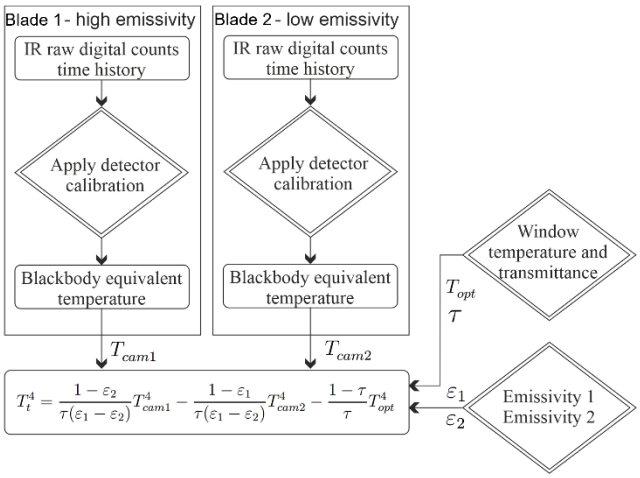

Figure 10 – Workflow to process IR data from raw digital counts to corrected target temperature.

Typical results and correction of blade tip temperature captured during a run in the OTRF are shown in Figure 11. The time histories are reported for a pixel on blade tip as marked with a star. The difference between the blackbody equivalent temperature of the high emissivity blade, T_{cam1}, and target temperature, T_t, provides the combined correction magnitude as a function of time. The correction increases from almost zero at near ambient conditions to approximately +5 K, or +1.23 %, at the end of the main test period when T_{cam1}~400 K.

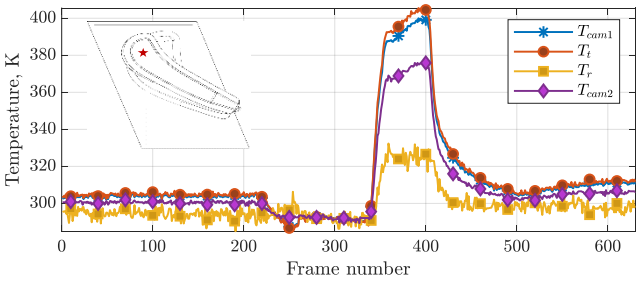

Figure 11 – Typical traces of temperature captured with IR camera in the OTRF and relative corrections.

A typical measurement of blade tip surface temperature for a single frame (392) with uniform turbine inlet conditions is shown in Figure 12(a). Data was acquired with a camera integration time of 5 µs. The tip features are clearly distinguishable with minimal blur and target velocity of almost 300 ms^{-1}. Corresponding data for RTDF inlet conditions are shown in Figure 13(a), with a similar temperature

distribution and general flow features are observed though with some differences in level that are considered later. For both inlet conditions, higher surface temperature along the pressure side rim, followed by a sharp decrease upon entering the tip cavity, is evidence that the flow separates on entry to the squealer cavity and a recirculation zone forms behind the pressure side rim. In the upstream zone of the squealer cavity, closer to the blade leading edge, the flow reattaches leading to high temperature and high heat transfer. Moving towards the trailing edge, the cavity narrows reducing the area of flow reattaching, until at the trailing edge the width of the cavity is so narrow that the flow does not reattach.

The impulse response method [41] was employed to process the measurement of temperature to heat flux $\dot{q}(t)$, under the assumption of semi-infinite substrate. Evaluation of heat flux allowed the regression to adiabatic wall temperature T_{aw}.

Processed data of adiabatic wall temperature over the blade tip for uniform and RTDF inlet conditions are shown in Figure 12(b) and Figure 13(b) respectively, providing interesting insight. Towards the leading edge and within the cavity gutter a decrease in adiabatic wall temperature is observed for RTDF inlet condition. Similar behaviour was seen by Qureshi et al. [28] on the rotor casing, driven by changes in local gas temperature – see spanwise analysis in Figure 14(b). In contrast, the adiabatic wall temperature is seen to increase along the pressure side rim. This is likely driven by hot gas migration on the blade pressure surface transporting hot gas – with a temperature hotter than the inlet mean – from nearer mid-span into the tip leakage flow. This behaviour can have a significant impact on blade life. Once this flow separates on entry into the cavity it mixes with colder gas within the recirculation zone. Finally, the data is presented as Nusselt number based on a reference length as defined in the following equation:

$$Nu_{T_{aw}} = \frac{\dot{q}(t)\, c_{true}}{k(T_{aw} - T_t(t))}$$

where c_{true} is the blade true chord used as reference length, k is the air thermal conductivity, T_{aw} is the adiabatic wall temperature, and T_t is the surface temperature measured by the IR camera. To the best of the authors' knowledge, this is the first instance of fully spatially resolved Nusselt number measurements on a high-pressure turbine blade tip conducted in an engine-representative rotating facility.

Comparing the determined Nusselt number over the tip for the two inlet conditions, depicted in Figure 12(c) and Figure 13(c) respectively, allows comparison of convective heat transfer coefficients. For both inlet conditions, distributions are similar with highest heat transfer coefficients in the reattachment zone. This agrees within past evidence that the effects of temperature distortion are driven by changes in local driving temperature rather than heat transfer coefficient. However, in this case a significant reduction in Nusselt number is seen at the leading-edge region of the tip, followed by a sharp increase. This may result from significant off-loading at the blade leading edge at the tip within the introduction of the radial temperature. Munk and Prim [42] suggested that temperature distortion does not affect the aerodynamic flow field in a static vane, later experimentally demonstrated by Butler et al. [25]. However, variation in local gas temperature at vane exit results in changes in local acoustic velocity, which along with a consistent absolute flow angle at vane exit results in relative flow angle changes at rotor inlet with the introduction of RTDF. Based on this behaviour, the influence of RTDF introduction on the rotor inlet relative flow

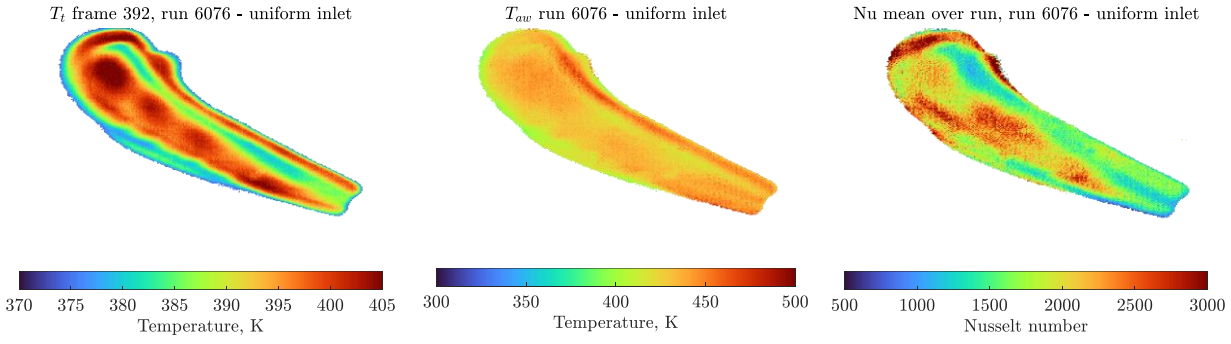

(a) (b) (c)

Figure 12 – Results on the rotor blade tip for uniform inlet condition: (a) single frame surface temperature, (b) adiabatic wall temperature, and (c) Nusselt number. Camera iteration time – 5 µs.

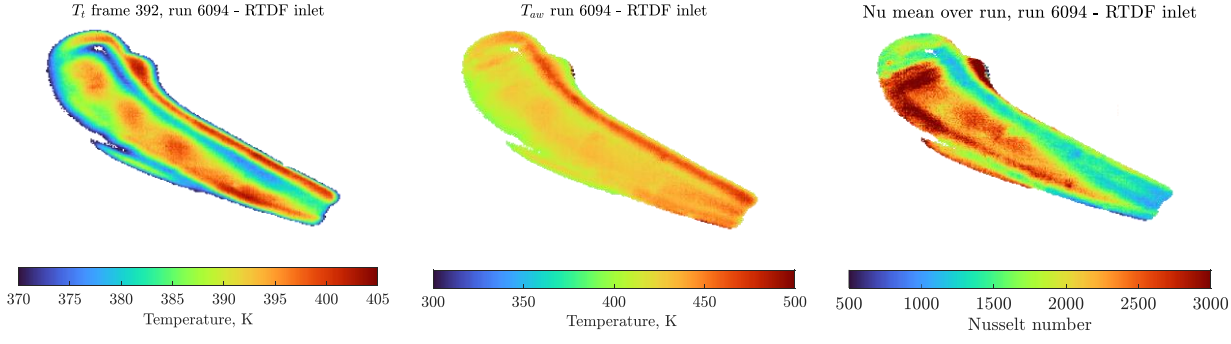

(a) (b) (c)

Figure 13 – Results on the rotor blade tip for RTDF inlet condition (a) single frame surface temperature, (b) adiabatic wall temperature, and (c) Nusselt number. Camera iteration time – 5 µs.

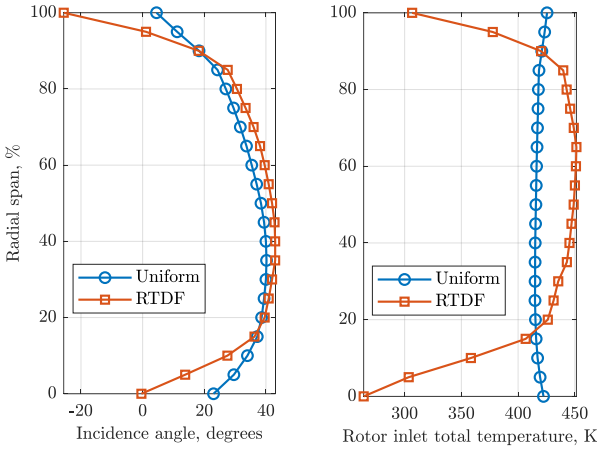

Figure 14 – Predicted spanwise changes in rotor inlet relative flow angle and total temperature.

angle and total temperature are analysed in Figure 14. Towards the blade tip, much reduced local gas temperature reduces the vane exit acoustic velocity, and consequently the absolute flow velocity given constant Mach number, resulting in changes to rotor incidence of approximately -10° and -30° at 95% and 100% radial span respectively. This causes the rotor stagnation line to move towards the suction side and the high Nusselt number region in Figure 13(c).

Figure 15 and Figure 16 illustrate the results of the heat transfer experiments over the blade pressure surface at uniform and RTDF inlet conditions, respectively. Data at uniform inlet condition was acquired with a camera integration time of 5 µs, while data at RTDF conditions is shown at 1 µs due to a corruption of the 5 µs dataset. Data at 1 µs was also collected to assess effect of iteration time (discussed in [40]). The shorter integration time results in sharper edges but introduces more noise and higher errors. Ignoring uncertainties from blur, errors at 5 µs were quantified as 1%, while at 1 µs, errors were 1.5% for temperatures of 400 K. With RTDF inlet, noticeable increases in surface temperature for a particular time instant are observed, that are also seen in the derived results of adiabatic wall temperature. This agrees with the measurements of Butler et al. [25] and Qureshi et al. [28] and can be explained by the hot gas segregation effect. Hot gas on the pressure surface migrates over the pressure surface, into the tip leakage flow, supporting the proposed mechanism for the increased adiabatic wall temperature measured on the pressure side squealer tip rim with RTDF inlet. The Nusselt number distributions in Figure 15(c) and Figure 16(c) are comparable, confirming first order changes in adiabatic wall temperature are driven by changes in driving gas temperature rather than heat transfer coefficient.

To demonstrate a major advantage of the IR measurement technique, heat transfer results acquired using traditionally-used thin film gauges with uniform inlet conditions at 80% radial span on the blade pressure surface are presented in Figure 18 for comparison with results using IR thermography at the same location shown in Figure 17. Using platinum thin film gauges sputtered on 50 µm Kapton, the thermal pulse quickly reaches the aluminium blade substrate resulting in a temperature trace that remains approximately flat during the stable portion of the run. This behaviour, commonly encountered with thin-film gauges measurements on rotor blade in transient turbine test facilities, arises from the inability of the gauge substrate to manifest adequate insulation and precludes the use of the regression technique to calculate the adiabatic wall temperature.

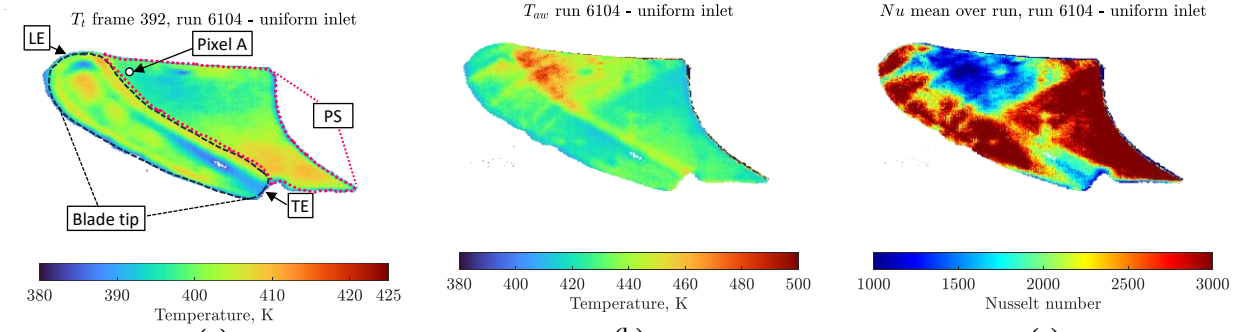

Figure 15 – Results on the rotor blade pressure surface for uniform inlet condition: (a) single frame surface temperature, (b) adiabatic wall temperature, and (c) Nusselt number. Camera iteration time – 5 µs.

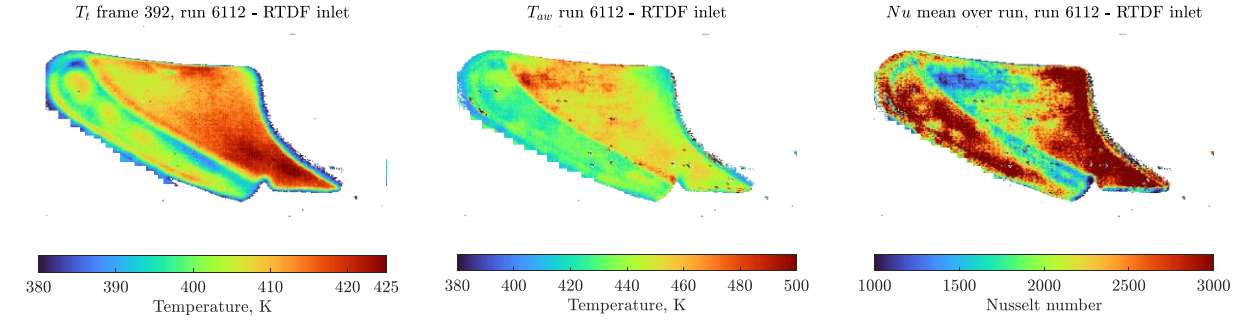

Figure 16 – Results on the rotor blade pressure surface for RTDF condition: (a) single frame surface temperature, (b) adiabatic wall temperature, and (c) Nusselt number. Camera iteration time – 1 µs.

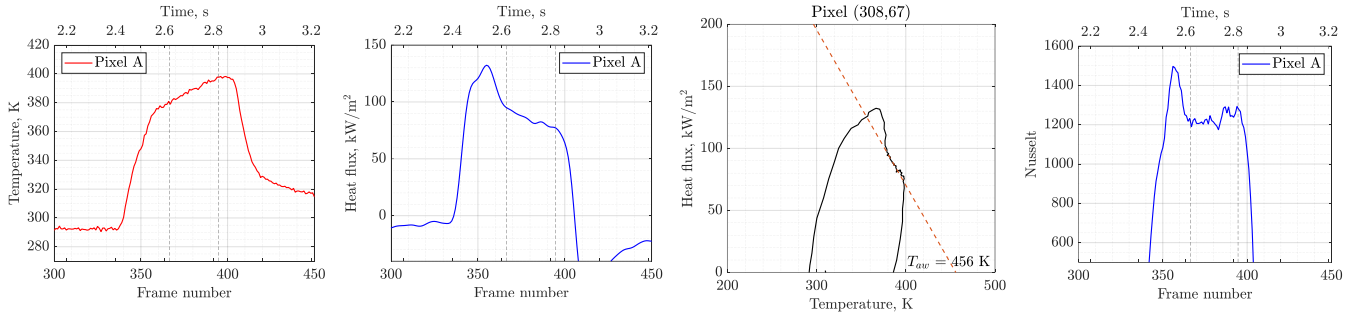

(a) (b) (c) (d)

Figure 17 – Results for one pixel on the blade pressure side for uniform inlet conditions: (a) surface temperature history (b) heat flux reconstructed from measured temperature; (c) adiabatic wall temperature extrapolation; (d) Nusselt number.

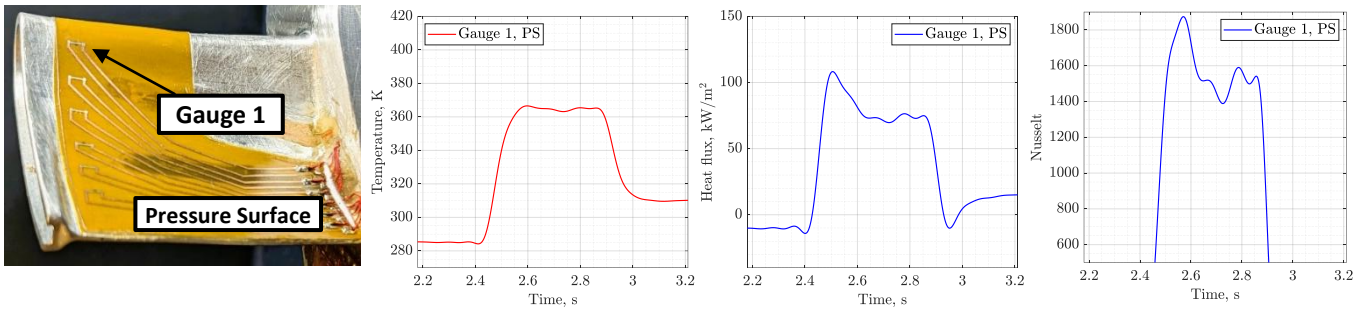

(a) (b) (c) (d)

Figure 18 – Results for uniform inlet condition from gauge 1 on the blade pressure side. Including (a) photograph of blade; (b) measured temperature; (c) heat flux reconstructed from measured temperature; (d) Nusselt number obtained with relative temperature and blade chord at 80% span.

A common practice (for example Qureshi et al. [28]) is to process heat flux to Nusselt number assuming the relative total temperature to equal the local driving temperature for heat transfer:

$$Nu_{T_{02,rel}} = \frac{\dot{q}(t)\, c_{true}}{k\left(T_{02,rel} - T_w(t)\right)}$$

where $T_w(t)$ is the wall temperature from the thin-film gauges, $\dot{q}(t)$ is heat flux deduced from $T_w(t)$, and $T_{02,rel}$ is calculated based on the design angles and velocity triangles at the specific span. The thermal conductivity of air, k, is evaluated at $T_{02,rel}$. Both representations of Nusselt number are approximately flat during the test window, with an average value of 1496 from the thin-film gauges and 1250 from the IR thermography, agreeing to within ±16%.

Consequently, thin-film gauge data on the blade surface in the OTRF has always been limited to validation of CFD, rather than allowing processing to adiabatic wall temperature and a Nusselt number that can be scaled to engine conditions. The developed IR system overcomes this issue and enabled measurement of adiabatic wall temperature on the rotor, a ground-breaking accomplishment not previously achieved.

4 Computational Validation

An available unsteady 3D CFD simulation developed using the Rolls-Royce Hydra solver to explore the effect of effusion cooling in the turbine rotor overtip region (not discussed in this paper) was used in an attempt to give further confidence to the novel experimental measurements.

4.1 HYDRA CFD Model

The CFD domain, shown in Figure 19, extended from the rotor inlet to the rotor exit plane, encompassing two rotor blades and the rotor overtip casing. Full resolution of the casing effusion holes required the introduction of sliding plane interface within the rotor tip gap to capture the combined effect of the moving rotor and the stationary casing. The CFD domain was therefore divided into two sub-domains: the HPT rotor and the casing, respectively.

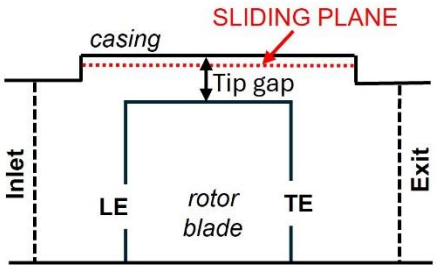

Figure 19 – Schematic of the computational domain.

The CFD domains were meshed using BOXER, an unstructured meshing commercial software developed by Cambridge Flow solutions Ltd. The meshing strategy was informed through previous mesh accuracy and grid independence studies [43] [44].

The computational domain comprised a total of 47.5 million cells, 32.5 million for the rotor blade domain and 15 million for the casing domain. Figure 20(a) present a sectional cut of the mesh showing the refined blade wake. To reduce the domain size, refinements were mostly focused on the key regions for the effusion cooling studies, which included the blade tip, the tip gap, and the overtip casing. This resulted in a global near wall y+ below 4 as displayed in Figure 20(b). Consequently, comparison to experiment was limited to the blade tip where the near wall y+ was approximately unity.

The measured temperature traverse at HP NGV inlet was

implemented in the Rolls-Royce throughflow solver Q263 with mixing factors applied so that the rotor inlet temperature radial profile could be matched to stage CFD prediction. Subsequently the throughflow predicted temperature profile was used in the rotor only unsteady CFD analysis. Radial profiles of total pressure, temperature, flow angles, and turbulence were used as boundary conditions at the rotor inlet, whilst a profile of static pressure was used at the rotor exit. The latter was also matched with the experimentally measured profile. The different types of boundary conditions used in the simulation are summarised in Table 1.

The solutions of the CFD simulation were obtained using the Rolls-Royce density-based in-house solver HYDRA, which is based on preconditioned time marching of the Reynolds Averaged Navier-Stokes (RANS) equations [45]. The governing flow equations are discretised in space using a second-order edge-based finite volume scheme-based flux differencing algorithm and integrated in time using a 5-stage Runge–Kutta scheme. The k-ω shear stress transport model was employed for turbulence closure. Wall functions were imposed on the solid boundaries and perfect gas behaviour was assumed. The implicit dual time-stepping with a physical time step of 3.50 µs was used to perform unsteady nonlinear calculations. The unsteady CFD models were initialised with steady state solutions and run with 150-time steps per rotor passing event, until the time periodic solution was obtained. Convergence was measured by monitoring local flow quantities, e.g. static pressure at the tip gap region, on the blade and the casing until a stable behaviour was reached throughout every blade passing event.

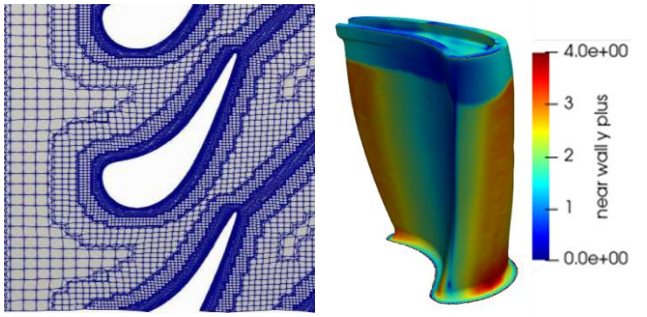

(a) (b)

Figure 20 – (a) BOXER mesh around blade tip and wake regions, (b) Contours of wall y+ for the blade surface.

Table 1: Boundary condition types used for CFD simulation.

Station	Boundary Condition
Domain inlet	Subsonic inflow
All walls	Viscous walls
Blade/casing interface	Sliding plane
Domain exit	Non-reflecting subsonic outflow

4.2 Computational Results

Adiabatic wall temperature predictions on the rotor tip with uniform inlet conditions obtained from HYDRA CFD simulations are shown in Figure 21(a). The experimental result are re-plotted in Figure 21(b) for ease of comparison. Likewise, simulation and experimental results of adiabatic wall temperature on the blade tip with RTDF inlet are shown in Figure 22. In general, an excellent agreement is found between the flow features observed in the results with both inlet conditions. Both CFD and experiment depict: (i) higher adiabatic wall temperature along the pressure side rim, (ii) a cooler suction side rim, (iii) enhanced pressure side rim temperature with the introduction of RTDF, and (iv) reduced temperature in the cavity and along suction rim with the introduction of RTDF. Comparing levels, experiment data show slightly higher values compared to CFD. For instance, for the uniform inlet conditions case the experimental results of adiabatic wall temperature range from 387 K to 479 K, compared to the 372 K to 459 K predicted with CFD. This discrepancy (~20 K) agrees with that observed between CFD and thin film experimental data acquired on the stationary casing wall above the rotor tip with effusion cooling of 15 K. This data cannot be shown here due to UK Government Security Classification.

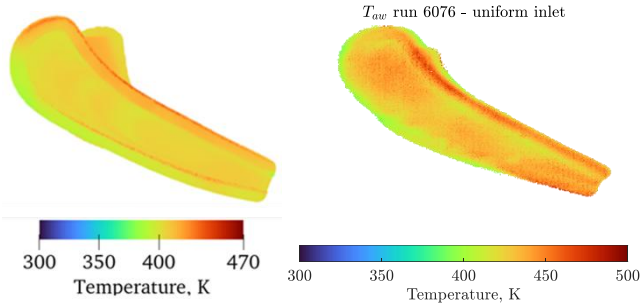

(a) (b)

Figure 21 – Adiabatic wall temperature on blade tip with uniform inlet condition from: (a) HYDRA CFD, (b) Experiment (IR thermography).

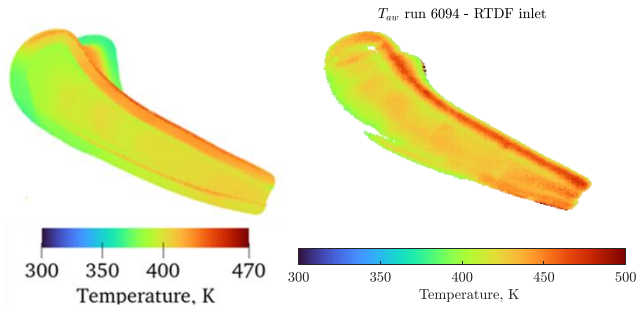

(c) (d)

Figure 22 – Adiabatic wall temperature on blade tip with RTDF inlet condition from: (a) HYDRA CFD, (b) Experiment (IR thermography).

5 Conclusions

The impact of temperature distortions on the heat transfer of the high-pressure rotor blades have been investigated in the Oxford Turbine Research Facility at engine matched conditions. Experiments were conducted using a uniform and a radial temperature profile, focusing on a blade with squealer tip. The radial temperature profile simulated conditions representative of rich-burn combustor in real engine operation. Infrared thermography was used to detail heat transfer measurements. The significance of the experimental data lies in having spatially resolved the heat transfer analysis on the rotor blade tip, obtaining two-dimensional maps of adiabatic wall temperature and Nusselt number, which had not been achieved in a turbine rotating facility before.

The main experimental findings are as follows:

a) Flow features in the squealer tip

For both uniform and RTDF conditions, higher surface temperatures were observed along the pressure side rim. A sharp temperature drop at the cavity entrance confirmed flow separation and the formation of a recirculation vortex behind the pressure side rim. Flow reattaches in the upstream squealer cavity near the leading edge but the reattachment region is reduced as the cavity narrows toward the trailing edge, where the flow remains fully separated.

b) Blade tip adiabatic wall temperature

In presence of the temperature distortion, a decrease in adiabatic wall temperature was observed towards the leading edge and within the cavity, a behaviour driven by changes in local gas temperature. In contrast, the adiabatic wall temperature was seen to increase along the pressure side rim, driven by hot gas migration on the blade pressure surface transporting hot gas from nearer mid-span into the tip leakage flow. This behaviour can have a significant impact on blade life. Once this flow separates on entry into the cavity it mixes with colder gas within the recirculation zone.

c) Blade tip Nusselt number

For both inlet conditions, heat transfer was highest in the reattachment zone, confirming that effects of temperature distortion are driven by local driving temperature rather than heat transfer coefficient changes. A significant reduction in Nusselt number was seen at the leading-edge region of the tip, followed by a sharp increase. This can be explained by a significant off-loading at the blade leading edge at the tip within the introduction of the radial temperature. The influence of RTDF introduction on the rotor incidence resulted in predicted changes of approximately -10° and -30° at 95% and 100% radial span respectively.

d) Blade pressure surface

With RTDF inlet, noticeable increases in surface temperature for a particular time instant were observed, that are also seen in the derived results of adiabatic wall temperature. This can be explained by the hot gas segregation effect, supporting the proposed mechanism for the increased adiabatic wall temperature measured on the pressure side squealer tip rim with RTDF inlet. The Nusselt number distributions were comparable, confirming that first order changes in adiabatic wall temperature are driven by changes in driving gas temperature rather than heat transfer coefficient.

e) Infrared measurements validation

The comparison between thin-film gauges and infrared thermography measurements on the blade pressure surface demonstrated the ability of the latter to obtain a Nusselt number that can be scaled to engine conditions, in contrast to the one obtained with the former which has always been limited to validation of CFD. A simulation run with HYDRA gave further confidence in the measurements, as the distribution of the blade tip adiabatic wall temperature numerically predicted was found in agreement with the experimental result.

Nomenclature

Abbreviations

HP	High Pressure
NGV	Nozzle Guide Vane
$OTRF$	Oxford Turbine Research Facility
$RTDF$	Radial Temperature Distortion Factor
$SILOET$	Strategic Investment in Low-Carbon Technology
IR	Infrared
$FPGA$	Field Programmable Gate Arrays
$PEEK$	PolyEtherEtherKetone
CFD	Computational Fluid Dynamics
PS	Pressure surface
SS	Suction surface

Romans

T	Temperature, K
p	Pressure, Pa
N	Rotational speed, rpm
x	Penetration depth, m
t	Time, s
c	Chord, m
k	Thermal conductivity, W m^{-1} K^{-1}
$\dot{q}$	Heat flux, W m^{-2}
Nu	Nusselt number

Greek

α	Material diffusivity, m^2 s^{-1}
ε	Emissivity
τ	Transmissivity

Subscripts

0	Stagnation conditions
1	NGV inlet
2	Rotor inlet
3	Rotor exit
eff	Effectiveness
h	Hot stream
0	Stagnation conditions
c	RTDF cold flow
$cam1$	Camera blade 1
$cam2$	Camera blade 2
t	Target value
opt	Optical path
r	Reflected value
aw	Adiabatic wall
w	Wall value
rel	Relative value

6 References

[1] M. Sisti, C. Falsetti and P. F. Beard, "Infrared temperature measurements on fast moving targets: A novel calibration approach," *Measurement,* vol. 225, p. 113870, 2024.

[2] J. Han, "Advanced Cooling in Gas Turbines 2016 Max Jakob Memorial Award," *Journal of Heat Transfer,* p. 140(11):113001, 2018 .

[3] X. Guo, W. Zheng, C. Xiao, L. Li, S. Antonov, Y. Zheng and Q. Feng, "Evaluation of microstructural degradation in a failed gas turbine blade due to overheating," *Engineering Failure Analysis,* vol. 103, pp. 308-318, 2019.

[4] D. E. Metzger, M. G. Dunn and C. Hah, "Turbine Tip and Shroud Heat Transfer," in *Gas Turbine and Aeroengine Congress and Exposition*, Brussels, Belgium, 1990.

[5] R. S. Bunker, "A Review of Turbine Blade Tip Heat Transfer," *Annals of the New York Academy of Sciences*, vol. 934, pp. 64-79, 2001.

[6] B. Sunden and G. Xie, "Gas Turbine Blade Tip Heat Transfer and Cooling: A Literature Survey," *Heat Transfer Engineering*, vol. 31(7), p. 527–554, 2010.

[7] J. P. Bindon, "The Measurement and Formation of Tip Clearance Loss," *ASME Journal of Turbomachinery*, vol. 111, pp. 257-263, 1989.

[8] T. Arts and V. K. I. for Fluid Dynamics, Turbine Blade Tip Design and Tip Clearance Treatment: January 19-23, 2003, Von Karman Institute for Fluid Dynamics, 2004.

[9] R. Bunker, "Axial Turbine Blade Tips: Function, Design, and Durability," *Journal of Propulsion and Power*, pp. 22:2, 271-285, 2006.

[10] J. S. Zainab, J. A. Eldad and K. Theodosios, "Effect of in-service burnout effect on the transonic leakage flows over cavity tip model," in *Proceedings of the Institution of Mechanical Engineers, Part A: Journal of Power and Energy*, 2021.

[11] A. A. Ameri, E. Steinthorsson and D. L. Rigby, "Effect of Squealer Tip on Rotor Heat Transfer and Efficiency," in *Proceedings of the ASME 1997 International Gas Turbine and Aeroengine Congress and Exhibition*, 1997.

[12] M. K. Chyu, H. K. Moon and D. E. Metzger, "Heat Transfer in the Tip Region of Grooved Turbine Blades," *ASME Journal of Turbomachinery*, vol. 111, pp. 131-138, April 1989.

[13] F. J. G. Heyes, H. P. Hodson and G. M. Dailey, "The Effect of Blade Tip Geometry on the Tip Leakage Flow in Axial Turbine Cascades," in *Proceedings of the ASME 1991 International Gas Turbine and Aeroengine Congress and Exposition*, 1991.

[14] G. S. Azad, J. C. Han, S. Teng and R. J. Boyle, "Heat Transfer and Pressure Distributions on a Gas Turbine Blade Tip," *Journal of Turbomachinery*, vol. 122, pp. 717-724, February 2000.

[15] G. S. Azad, J. C. Han and R. J. Boyle, "Heat Transfer and Flow on the Squealer Tip of a Gas Turbine Blade," *ASME Journal of Turbomachinery*, vol. 122, pp. 725-732, 2000.

[16] J. S. Kwak, J. Ahn, J. C. Han, C. P. Lee, R. S. Bunker, R. Boyle and R. Gaugler, "Heat Transfer Coefficients on the Squealer Tip and Near-Tip Regions of a Gas Turbine Blade With Single or Double Squealer," *ASME Journal of Turbomachinery*, vol. 125, pp. 778-787, 2003.

[17] F. Didier, R. Dénos and T. Arts, "Unsteady Rotor Heat Transfer in a Transonic Turbine Stage," *ASME Journal of Turbomachinery*, vol. 124, no. 4, pp. 614-622, 2002.

[18] M. Dunn and C. Haldeman, "Time-Averaged Heat Flux for a Recessed Tip, Lip, and Platform of a Transonic Turbine Blade," *ASME Journal of Turbomachinery*, vol. 122, no. 4, pp. 692-698, 2000.

[19] S. Thorpe, S. Yoshino, G. Thomas, R. Ainsworth and N. Harvey, "Blade-tip heat transfer in a transonic turbine," in *Proceedings of the Institution of Mechanical Engineers, Part A: Journal of Power and Energy*, 2005.

[20] L. Christensen, R. Celestina, S. Sperling, R. Mathison, H. Aksoy, J. Liu and J. Nickol, "Comparison of Computational Predictions for a Cooled High-Pressure Turbine to Data From a Short Duration Experiment," in *Turbo Expo: Power for Land, Sea, and Air*, 2023.

[21] D. Dorney, K. Gundy-Burlet and D. Sondak, "A Survey Of Hot Streak Experiments And Simulations," *International Journal of Turbo and Jet Engines*, pp. 16(1), 1-16, 1999.

[22] T. Povey and I. Qureshi, "Developments in Hot-Streak Simulators for Turbine Testing," *ASME. Journal of Turbomachinery*, vol. 131, no. 3, p. 031009, July 2009.

[23] T. Shang, G. Guenette, A. Epstein and A. Saxer, "The influence of inlet temperature distortion on rotor heat transfer in a transonic turbine," in *31st AIAA/ASME/SAE/ASEE Joint Propulsion Conference and Exhibit*, San Diego, CA, 1995.

[24] T. Shang and A. H. Epstein, "Analysis of Hot Streak Effects on Turbine Rotor Heat Load," *ASME Journal of Turbomachinery*, vol. 119, no. 3, pp. 544-553, 1997.

[25] T. L. Butler, O. P. Sharma, H. D. Joslyn and R. P. Dring, "Redistribution of an inlet temperature distortion in an axial flow turbine stage," *Journal of Propulsion and Power*, vol. 5, no. 1, pp. 64-71, 1989.

[26] K. S. Chana and T. V. Jones, "An Investigation on Turbine Tip and Shroud Heat Transfer," *ASME Journal of Turbomachinery*, vol. 125, no. 3, pp. 513-520, 2003.

[27] P. F. Beard, A. Smith and T. Povey, "Impact of Severe Temperature Distortion on Turbine Efficiency," *ASME Journal of Turbomachinery*, vol. 135, no. 1, p. 011018 (12 pages), 2013.

[28] I. Qureshi, A. D. Smith, K. S. Chana and T. Povey, "Effect of Temperature Nonuniformity on Heat Transfer in an Unshrouded Transonic HP Turbine: An Experimental and Computational Investigation," *ASME Journal of Turbomachinery*, vol. 134, p. 011005, May 2011.

[29] C. Falsetti, P. F. Beard, D. N. Cardwell and K. S. Channa, "A Review of High-Speed Rotating HP Turbine Heat Transfer and Cooling Studies Over the Last Decade in the Oxford Turbine Research Facility," in *ASME Turbo Expo 2022*, Rotterdam, 2022.

[30] S. Shahpar and S. Caloni, "Aerodynamic Optimization of High-Pressure Turbines for Lean-Burn Combustion System," *ASME Journal of Engineering for Gas Turbines and Power*, vol. 135, p. 055001, April 2013.

[31] P. Beard, On Transient Turbine Efficiency Measurements with Engine Representative Inlet Flows, Oxford: DPhil Thesis, 2010.

[32] M. G. Adams, T. Povey, B. F. Hall, D. N. Cardwell, K. S. Chana and P. F. Beard, "Commissioning of a Combined Hot-Streak and Swirl Profile Generator in a Transonic Turbine Test Facility," *ASME Journal of Engineering for Gas Turbines and Power,* vol. 142, pp. 031008-1-16, 2020.

[33] D. Singh, P. F. Beard, D. N. Cardwell and K. S. Chana, "Investigation of a High-Pressure Turbine Stage in a High-Speed Rotating Transient Test Facility for Rotor Tip Study and a Parametric Study for Improved Heat Transfer Calculation," *ASME Journal of Turbomachinery,* vol. 144, no. 12, p. 121020 (13 pages), 2022.

[34] D. Singh, P. F. Beard, D. Cardwell, V. Starlens, P. Bahulekar, M. Stokes, S. Bather and K. S. Chana, "An Aerodynamic Investigation of a High-Pressure Turbine Using Rotor Casing Static Pressure Measurements at Engine Repre-sentative Conditions With Different Tip Designs, Tip Gaps, and Inlet Temperature Profiles," *ASME Journal of Turbomachinery,* vol. 147, no. 6, p. 15, 2025.

[35] M. Sisti, A Novel Infrared Thermography Technique for Measuring Heat Transfer in Transonic Turbine Blades, Oxford: DPhil Thesis, 2024.

[36] M. Sisti, C. Falsetti, P. F. Beard and K. Chana, "Infrared temperature measurements on high pressure turbine blades in the Oxford Turbine Research Facility: calibration and image processing techniques," in *Proceedings of 14th European Conference on Turbomachinery Fluid dynamics & Thermodynamics*, 2021.

[37] D. Schultz and T. Jones, "Heat-transfer measurements in short duration hypersonic facilities," *AGARD-AG-165,* vol. AG(165), 1973.

[38] M. Collins, K. Chana and T. Povey, "New technique for the fabrication of miniature thin film heat flux gauges," *Measurement Science and Technology,* vol. 26, no. 2, p. 025303, 2015.

[39] R. Anthony, M. Oldfield, T. Jones and J. LaGraff, "Development of high-density arrays of thin film heat transfer gauges," in *Proceedings 5th ASME/JSME Thermal Engineering Joint Conference*, San Diego, CA, 1999.

[40] M. Sisti, C. Falsetti and P. F. Beard, "High Speed infrared thermography measurement applied to transonic turbine rotor in an engine scale rotating facility," *Measurements, paper under review,* 2025.

[41] M. L. G. Oldfield, "Impulse Response Processing of Transient Heat Transfer Gauge Signals," *ASME Journal of Turbomachinery,* vol. 130, 2008.

[42] M. Munk and R. C. Prim, "On the Multiplicity of Steady Gas Flows Having the Same Streamline Pattern," in *Proceedings of the National Academy of*, 1947.

[43] P. Beard, M. Adams, J. Nagawakar, M. Stokes, F. Wallin, D. Cardwell, T. Povey and K. S. Chana, "The LEMCOTEC 1½ Stage Film-Cooled HP Turbine: Design, Integration and Testing in the Oxford Turbine Research Facility," in *13th European Conference on Turbomachinery Fluid Dynamics and Thermodynamics*, 2019.

[44] G. Zamboni and P. Adami, "On the Unsteady Interaction Between the Leakage and the Main Passage Flow in a High Pressure Turbine Rig: CFD URANS Investigations and Comparison With the Rig Test Data," in *Proceedings of the ASME Turbo Expo 2016: Turbomachinery Technical Conference and Exposition*, Seoul, South Korea, 2016.

[45] L. Lapworth, "Hydra-CFD: a framework for collaborative CFD development," in *International conference on scientific and engineering computation (IC-SEC)*, 2004.